Health monitoring in continuous glass fibre reinforced thermoplastics: Manufacturing and application of interphase sensors based on carbon nanotubes

J. Rausch, E. Mäder

Accepted Manuscript

Health monitoring in continuous glass fibre reinforced thermoplastics: Manufacturing and application of interphase sensors based on carbon nanotubes

J. Rausch, E. Mäder

PII: S0266-3538(10)00202-2
DOI: 10.1016/j.compscitech.2010.05.018
Reference: CSTE 4723

To appear in: *Composites Science and Technology*

Received Date: 25 February 2010
Revised Date: 11 May 2010
Accepted Date: 23 May 2010

Please cite this article as: Rausch, J., Mäder, E., Health monitoring in continuous glass fibre reinforced thermoplastics: Manufacturing and application of interphase sensors based on carbon nanotubes, *Composites Science and Technology* (2010), doi: 10.1016/j.compscitech.2010.05.018

Health monitoring in continuous glass fibre reinforced thermoplastics: Manufacturing and application of interphase sensors based on carbon nanotubes

J. Rausch, E. Mäder*

Dept. of Composites, Leibniz Institute of Polymer Research Dresden, Hohe Strasse 6, 01069 Dresden, Germany

Abstract

In this study, a new approach for health monitoring of GF reinforced composites is presented by incorporating percolated carbon nanotubes (CNTs) into the composites interphase. This is achieved applying CNT-filled coatings to glass fibres (GF). Taking advantage of the electrical properties of CNTs, this allows a highly localized monitoring of the composites interphase.

The approach is largely independent on matrix material and can be applied to thermoplastic or thermoset resin matrix materials with minor adjustments. The resistance of CNT-coated GF yarns shows a linear dependence on the yarn length and depends on the CNT weight fraction of the coating, as well as on the amount of coating on the GF yarn. Performing tensile tests in combination with simultaneous resistance measurements on CNT- coated GF yarns embedded in a polypropylene matrix, the interphase behaviour during mechanical loading is monitored, providing information on this specific area. This allows relating interphase failure or GF breakage to the resistance data and demonstrates the potential of this approach for health monitoring of GF reinforced composites.

Keywords: A. Carbon nanotubes; A. Glass fibres; B. Interphase; B. Electrical properties; Sensing

* Corresponding author. Tel.: +49 351 4658305; fax: +49 351 4658362.
E-mail address: emaeder@ipfdd.de

1. Introduction

Over the past several years there has been an increasing effort in developing strategies for health monitoring of fibrous composites [1-6]. Among the variety of different sensor concepts, the application of CNTs shows great potential for this purpose in composite materials. When the amount of CNTs exceeds the systems percolation threshold, a CNT network within the matrix is formed and any applied mechanical strain causes a dimensional change on the nano-scale. Thus, the electrical resistance is a function of the applied strain and allows to *in-situ* monitor the strain and the therewith possibly associated damage in the composite. As the extent of many defects in composite materials is in the sub-μm range, CNTs are well-suited for strain mapping on that scale due to their small dimensions.

Schulte et al. were the first in exploring the suitability of percolated CNT networks for health monitoring of continuous glass fibre/epoxy composites [7] and in the recent years numerous studies have followed dealing with different aspects of *in-situ* strain sensing by recording the change in electrical resistance upon variation of mechanical strain [8,9].The sensitivity of CNT networks with regard to the onset of matrix dominated failure and the failure propagation could be demonstrated [10,11] as well as the possibility to monitor the fatigue life of glass fibre (GF) reinforced epoxy composites [12]. The current state of research related to sensing with CNTs has been comprehensively reviewed by Chou et al. [13,14].

Most of the literature using CNTs for sensing of mechanical strain involves CNTs distributed throughout the bulk matrix. Consequently, any change in resistance may be related to any response of the CNT network in the bulk. However, as the mechanical performance of fibre reinforced composites is closely related to the fibre/matrix interface and its ability to transfer the applied stress from the bulk into the fibres, it is desirable to assess the interfacial strain separately from that of the bulk. In this context, interface strain mapping of GF/epoxy composites has already been performed by Raman spectroscopy relating certain band shifts to the externally applied strain [15-17].

In this study we present a new concept for health monitoring in GF reinforced composites by depositing multi walled CNTs within an aqueous coating onto the GF surface. Hence, the extension of the CNT network is restricted solely to the interphase,

which forms upon consolidation of the composite. Thus any change in electrical resistance can be regarded as a true interphase response rather than a bulk related phenomenon. We see the potential of this approach in its versatility: (i) as only the coating recipe needs to be modified, it can be tailored for improved adhesion strength adopted to either thermoplastic or thermoset matrices, respectively, without causing internal stress concentrations or additional interfaces, (ii) only very little volume of the composite contains CNTs, i.e. the absolute weight fraction of CNTs in the composite is very low compared to bulk nanocomposites, (iii) the GF yarns can be coated on a large scale employing industrial processing routes, (iv) single GF yarns can be introduced into macroscopic textile composites for surveillance purposes of highly stressed areas.

In the following, the manufacturing of CNT-coated yarns and their characterization with regard to their electrical resistance are described. Moreover, results of the tensile testing and the simultaneous recording of resistance change for a CNT-coated GF yarn embedded in polypropylene (PP) are presented.

2. Experimental

Multi-walled CNTs (NC3150, Nanocyl S.A., Belgium) were added to surfactant solution and treated with a horn sonicator for 120 min at constant output power of 40 W. The aqueous surfactant solution was prepared dissolving Brij76 (polyoxyethylene (10) stearyl ether; Sigma Aldrich) in deionised water. The surfactant to CNT ratio was adjusted to 1.5/1, using 0.3 wt% CNT in 100 ml deionised water. Throughout sonication of the batches with 100 ml, the beaker with the CNTs was cooled in a water bath.

In the next step, different quantities of pre-dispersed CNTs were added to a PP-film former. In order to homogenise the system, the pre-dispersed CNTs and the film former were magnetically stirred for several minutes. Afterwards, the system was freeze dried (Alpha 1-2 LD plus, Christ GmbH, Germany) and the obtained powder was used for compression moulding of thin films (K207, Rucks GmbH, Germany). In detail, the powder was heated from 25 °C to 200 °C with 15 K/min including a degassing step at 180 °C. After having reached 200 °C, the films were compression moulded at 30 bar for 2 min, before cooling down to 25 °C. As described elsewhere [18], volume resistivity measurements of the 80 μm thick films were carried out using a 4-point test fixture in

combination with the electrometers 6517a and DMM2000 (Keithley Instruments Inc.), respectively. The films were cut into pieces of about 30 x 25 mm and the through-thickness volume resistivity measured separately. The presented values are mean values of at least 4 measurements.

For preparation of the CNT-coated GF yarns, E-glass fibres with an average diameter of 15 µm were continuously spun and coated with an aqueous 1 wt% γ-aminopropyltriethoxysilane (APS) solution at the Leibniz Institute of Polymer Research Dresden. The yarn count of the GF filament yarn was 111 tex, containing 204 filaments. In a subsequent step the GF-yarns were coated with a CNT/film former system containing 0.5 wt% CNTs relative to the solid content of the film former on a horizontal vertical padder type HVF in combination with a continuous coating system type KTF (both Werner Mathis AG, Switzerland). The solid content of the CNT-coating on the GF yarns was determined by thermogravimetric analysis (TGA; Q500, TA Instruments). For obtaining images of the CNT-coated GF surfaces, a scanning electron microscope (SEM) Ultra 55 (Carl Zeiss SMT AG, Germany) was employed. Apart from the charge contrast image, all samples had been sputtered with a 5 nm thick platinum layer before SEM characterization. Prior to measuring the electrical resistance using a Keithley 6514 programmable electrometer, the yarns were annealed in an oven at 200°C for 15 min. Depending on the measured yarn length, the GF were contacted with electrically conductive silver paint at the corresponding distances. For each measurement length at least five GF yarns were measured.

For the preparation of the tensile specimens the CNT-coated GF yarns were embedded in polypropylene (PP; Borealis HG455 FB) and compression moulded (K207, Rucks GmbH, Germany). The computer controlled cycle under vacuum comprised a heating step from 25 °C to 225°C. 5 min after reaching this temperature a pressure of 30 MPa was applied for 1 min, before cooling down to 25 °C. The heating and cooling was performed with a rate of 15 K/min. Tensile specimens with the dimensions of 60x15x4 mm were cut out of the compression moulded PP plate containing the embedded GF yarns. The mould was prepared in a way that the direction of the yarn axis points along the center line of each specimen in tensile direction. As the yarn length was chosen to be longer than the specimen length of 60 mm, the overlapping GF

yarn could be contacted using electrically conductive silver paint. The tensile testing was conducted on a UPM Zwicki 2.5 (Zwick GmbH & Co KG, Germany) with a crosshead velocity of 1 mm/min. No additional extensometer was used due to the small gauge length of 20 mm. The change in resistance of the embedded GF yarn during tensile testing was recorded simultaneously to the tensile loading using a Keithley 6514 programmable electrometer. Figure 1 shows the scheme of a tensile specimen with an embedded GF yarn.

3. Results and Discussion

3.1. Modification of the polymeric film former system by dispersed CNTs

By adding pre-dispersed CNTs [19] to the aqueous film former, different CNT weight fractions within a GF coating can be adjusted. After the CNTs are homogenized within the polymeric film former they can be deposited onto the GF in a separate sizing or coating step. The polymeric film former can be regarded as a latex which provides one way for manufacturing CNT-nanocomposites [20-24] alternatively to melt processing [25-27] sonication [28,29] or calandering [30].

Aiming at electrically conductive interphases, it is desirable to know the percolation threshold of the film former/CNT system. This is achieved by removing the aqueous part of the CNT-coating and compression moulding of the resulting solid content into films. Different amounts of pre-dispersed CNTs were added to the film former and the volume resistivity of the films as a function of CNT weight fraction was determined. However, it has to be taken into account that due to differing compression moulding parameters, the resistivity of the films is not necessarily identical with the interphase resistivity, as the processing conditions are know to affect the systems resistivity [18]. Figure 2 shows the dependence of the resistivity on the CNT weight fraction for the PP film former/CNT system used. As expected, a significant drop in resistivity is observed after the percolation threshold of the system at around 0.1 wt% is exceeded and further addition of CNTs has only a minor effect on the resistivity values. Using the latex approach, a low percolation threshold as well as a low volume resistivity of 4.5 Ohm*cm at 3 wt.% are observed compared with melt processed PP nanocomposites [31-34]. Although the percolation threshold is known to be affected by various factors, e.g. aspect ratio of CNTs [35,36], CNT waviness [37-39], processing conditions [40-

42], the obtained results clearly demonstrate the potential of the aqueous film former systems for the deposition of CNT networks on GF.

3.2. Preparation and characterization of CNT-coated GF yarns

Based on the information presented in figure 2, for the coating of the yarns a system containing 0.5 wt% CNTs with regard to the solid content of the film former was chosen. The coating of the yarns allows a larger variation of the solid content on the GF, i.e. the amount of CNT-coating, than it is possible by sizing the GF directly in the spinning process. As determined by TGA measurements, the GF yarns prepared had a solid content of 5.5, 10.4, 14.5, 21.6, and 29.4 wt%, respectively.

Figure 3 shows SEM micrographs of the coated GF yarns. In figure 3a the CNT-coating on the surface of GF yarn with 5.5 wt% solid content can be seen. At a higher magnification (fig. 3b) the spherical shape of the PP film former particles as well as the therein dispersed CNTs become visible. From the SEM micrographs in figure 3a and 3b, respectively, it becomes evident that the GF surface is inhomogeneously covered by the film former system. Relatively large areas of the GF appear to be uncovered by the film former, while others are covered by a thin layer or show cluster-like structures. This illustrates the challenges of this approach: Theoretically, a very thin and homogeneous layer of the film former/CNT-system on the GF surface would be ideal, as this allows the formation of continuous conductive paths. However, when GF are sized or coated the surface can rarely be assumed to be homogeneously and completely covered by the sizing/coating. Hence, the amount of film former on the GF has to be increased until continuous and interconnected areas, rather than an island-in-the-sea topography, are formed and one can take advantage of the electrical properties of the CNTs forming a network on the GF surface. This means that higher film former contents on the fibres are necessary, compared with GF used as reinforcing fibres, where the solid content on the fibres is about 1 wt%.

In spite of the initial film former distribution after the coating process, the topography and homogeneity of the film former/CNT layer can be affected by annealing the GF yarns. Figure 3c depicts a GF with 5.5 wt% solid content on the fibre after being annealed at 200°C for 15 min. Although the solid content is similar to the GF shown in figure 3a, the topography is very different to the one of the as-coated fibres. The PP particles of the film former are molten and have wetted the GF surface. Thus, the

topography is levelled and the film former/CNT system covers the GF surface in a more continuous manner. The latter effect is most important as this supports the formation of continuous conductive paths within the film former/CNT system on the GF surface even for low solid contents. For the prepared GF yarns with higher solid contents of coating the strand integrity of the yarn is improved and the individual filaments are held together by the coating forming fibre bundles. After the annealing CNTs can hardly be observed sticking out the PP film on the GF. However, charge contrast imaging [42-45] enables one to derive information about the distribution of CNTs within the outermost layer of nanocomposites. Figure 3d visualizes the CNT network within the PP film former on a annealed GF employing the charge contrast imaging technique. It can be observed that the CNTs are both, well dispersed and distributed within the PP film former. A similar distribution and state of dispersion of CNTs can expected for all areas on the GF covered by the film former. Hence, in the case of interphase sensors based on CNT-networks on the GF surface, any change in electrical resistance as a function of applied stress involves information of all continuously connected areas on the GF covered with the CNT-coating as well as conductive paths between adjacent fibres. Whenever a single GF fails or the interfacial shear stress exceeds a critical limit and locally causes the interphase to fail this will be reflected in a permanent increase of resistance, as certain conductive paths cease to exist.

Figure 4 schematically illustrates the differences between an ideally coated GF surface and the coating pattern like it can be observed on real GF surfaces. Figure 4a shows the cross section of an ideally coated GF, with all coating being present as a homogeneous and thin layer covering the GF surface. The top view on the surface of an ideally coated GF in figure 4b depicts a coating layer with no inhomogeneities, neither in terms of surface coverage nor regarding the thickness of the layer. This is different for GF surfaces like they can be found after coating application in real life. The cross section of such a GF (figure 4c) is characterised by a inhomogeneous coating distribution on the GF surface. Besides the fact that not all coated areas are interconnected, the coating layer thickness varies to a certain extent. This results in an irregular coating pattern on the GF surface, as presented in figure 4d. However, homogeneous coating layers are crucial as only interconnected areas can form continuous conductive paths along the fibre surface, thus taking part in the charge transfer.

In figure 5 the dependence of the GF yarn resistance on its length is illustrated for varying amounts of CNT-coating on the GF. Firstly, one can observe that for an identical yarn length the resistance decreases with increasing solid content on the fibre. This is expected since the resistance of the yarn is given by

$$R_{yarn} = \rho_{coating} \cdot {}^{l}\!/\!_{A_{coat}} \cdot \qquad (1)$$

Taking the volume resistance, $\rho_{coating}$, as well as the yarn length, l, as constant, an increasing amount of CNT-coating is related to an increase of the cross-sectional area, A_{coat}, of the CNT-coating in the GF yarn. However, an exact value for A_{coat} can not be provided since it has not a geometrically defined shape. Moreover, the thickness of the coating layer varies locally, thus A_{coat} is not identical for the whole measurement length. For the different amounts of CNT-coating on the GF yarns, distinct resistances are observed. For all GF yarns with coating contents >10 wt.%, the resistances range between several hundreds of kOhm for 5 cm yarn length and 10 MOhm for 30 cm yarn length, respectively. The GF yarn with 5.5 wt% CNT-coating lies well above that range between 15 and 86 MOhm. Moreover, it is noteworthy that the standard deviation becomes bigger for the yarns with lower coating content, which is related to inhomogeneities of the coating layers on the fibres. For higher coating contents on the GF it is more likely that besides all inhomogeneities in thickness a continuous layer is formed providing continuous conductive paths on the fibre surface, whereas for lower coating contents a growing percentage of the film former is not connected to the continuous structure of the film former and therefore does not contribute to the charge transfer. Similarly to this, the increase of the standard deviation with increasing measurement length is related to statistically distributed inhomogeneities in the conductive layer along the measured length of the yarn (cf. fig.5 and table 1). These inhomogeneities can be regarded as a bottleneck for the charge transfer. Consequently, a reduced measurement length results in less scattered and lower resistance values, similarly to the effect of gauge length on the tensile strength of brittle fibres as a consequence of the statistical distribution of the critical flaws [46]. Furthermore, a pronounced linear dependence of the resistance on the yarn length can be observed as predicted by equation 1. A linear least square fit through the origin was performed in order to derive the different slopes of the data sets. As expected, the smallest slope is found for the yarn with the highest coating content and a clear trend to steeper slopes with decreasing amount of CNT-coating on the yarn is observed. The differences between the yarns with 14.5, 21.6, and 29.4 wt%, respectively, are relatively modest,

but the yarns with lower coating contents show a comparably pronounced increase in the slope. The data of figure 5 is summarized in table 1.

In order to calculate the volume resistance, $\rho_{coating}$, of the coating according to equation 1, one must define the cross sectional area of the coating for the multifilament yarn. The latter quantity can be estimated using simple geometric considerations and the experimentally determined coating content of the yarn. For sake of calculation it is necessary to convert the volume of a certain length of the multifilament yarn, V_{yarn}, into a single GF with an identical volume, V_{GF}.

$$V_{GF} = V_{yarn} = {}^{T}\!/_{d_{GF}} \cdot l \tag{2}$$

Here, for E-glass density, d_{GF}, the value of 2.56 g/cm^3 was used, while for the yarn count, T, the known values of the titer in g/1000m were used. Now, the formerly geometrically undefined cross sectional area of the coating in the multifilament yarn can be assumed forming a homogeneous layer on the single GF. For a GF with a known volume, the radius can be easily deduced considering its cylindrical shape. Once the equivalent radius is known, the cross sectional area of the GF, A_{equiv}, can be calculated and the experimentally determined coating content of the multifilament yarn is assumed to be present on the single GF forming a concentric circle with a certain thickness. The cross sectional area of the coated single GF is composed of two partial areas: the cross sectional area of the GF itself, A_{equiv}, and the additional cross sectional area due to the thickness of the coating layer, A_{coat}. Knowing A_{equiv}, the cross sectional area of the coating can be expressed as

$$A_{coat} = {}^{d_{GF}}\!/_{d_{coa}} \cdot M_{coat} \cdot A_{equiv} \tag{3}$$

using the density ratio of GF and coating, d_{GF}/d_{coat}, and the known solid content on the GF, M_{coat}. The estimation of the cross sectional area in equation 3 for different coating weight fractions in the multifilament yarns yields the missing quantity to be used in equation 1 for the calculation of the volume resistivity of the yarns.

In figure 6 the calculated values for the GF yarns with different coating weight fractions are shown. It can be seen that $\rho_{coating}$ does not change with the measured GF yarn length, which is reasonable since the volume resistivity is a materials property of the characterized system, i.e. the film former/CNT system. However, figure 6 shows a strong dependence of $\rho_{coating}$ on the CNT- coating weight fraction. For the yarn with

5.5 wt% coating content comparably high volume resistivities of almost 200 Ohm*cm are calculated, whereas the yarn with 10.4 wt.% coating content shows significantly lower values of around 45 Ohm*cm. Any further increase of the coating weight fraction of the yarn results only in minor decreases of the resistivity which levels off at around 30 Ohm*cm. The fact that $\rho_{coating}$ is not found to be constant and apparently depends on the coating weight fraction seems to be incorrect at first glance. However, bearing in mind that the calculated results relate to coated GF they are reasonable and provide additional information on the coated GF surface. Nonetheless, it should be pointed out that $\rho_{coating}$ has to be regarded as a constant value depending for the given system on the CNT weight fraction only (cf. figure 2). Here, the dependence of $\rho_{coating}$ on the coating weight fraction is related to the wetting of the GF by the coating system and the determination of the coating weight fraction by TGA. Irrespective of the coating content of the yarn, the coverage of the GF by the film former/CNT system can never be assumed to be perfectly homogeneous. However, for higher coating contents the inhomogeneities do not result in a high degree of discontinuous film former layers, whereas with lower coating contents an increasing part of the CNT-coating forms island-in-the-sea structures on the GF surfaces and is not involved in forming continuous conductive paths (cf. fig. 3a and fig. 4). As the calculation of the volume resistivity in figure 6 is based on the film former content determined by TGA measurements, the whole film former content is taken into account, including as well the discontinuous and isolated coating structures. For yarns with a lower coating weight fraction these structures are more abundant than for yarns with higher coating weight fractions, causing the experimentally determined coating contents to be higher than the effective coating weight fraction on the GF surface being involved in charge transfer. As a consequence, higher volume resistivities are calculated for the yarns with 5.5 and 10.4 wt% coating content, respectively. The deviation of the volume resistivity from its plateau value at approximately 30 Ohm*cm between 14.5 to 29.4 wt% can be interpreted as a measure for an increasing percentage of coating forming discontinuous areas on the GF surface and not being involved into charge transfer. For the CNT-coating used, approximately 15 wt% result in an almost continuous film former layer.

3.3. Tensile test of CNT-coated GF yarn embedded in PP

In order to verify the feasibility of the CNT-coating to be used as an interphase sensor on GF, the yarn with 14.5 wt% coating content was embedded in a PP matrix and

subjected to tensile loading. Figure 7 shows representative results of the mechanical characterisation, where the resistance was recorded simultaneously to load and displacement. Although the CNT affected volume is very low with regard to the specimen volume and its extension is restricted to the interphase only, a pronounced resistance change with increasing displacement can be observed. This change in resistance can be regarded as an indirect measure of the interphase strain. Similarly to bulk nanocomposites, the initial slope and resistance change at low strain levels are fairly small [10,12]. With increasing displacement the slope becomes gradually steeper until the resistance changes stepwise at a certain stress level. This point coincides with the appearance of first discontinuities in the stress-displacement curve as can be inferred from the inset in figure 7. The first local maximum of the stress curve corresponds to the onset of GF breakage, which is still well below the maximum stress of the sample and demonstrates the sensitivity of the approach with regard to the detection of the initial failure of the reinforcing fibres. Besides the stepwise resistance change, indirect information regarding the interphase strain can be deduced from the slope of the resistance change curve. Right before the first filaments fail and a stepwise increase of resistance change is observed the slope has reached a certain value which is characteristic for the applied CNT-coating formulation. Based on that information one can predict when the interphase is about to fail, although the exact location of the interphase failure can not be predicted. Nevertheless, as the fibre-matrix bonding can be assumed to be at the same level at any spot on the GF, the occurrence of a first interphase failure indicates that a critical interphase stress level has been exceeded and any further increase of the loading will cause additional failure.

The effect of various issues, e.g. CNT weight fraction of the coating, coating weight fraction of the yarn, on the sensitivity are currently under investigation and will be presented in a separate study.

4. Conclusions

A new approach for in-situ interphase strain sensing in continuously reinforced GF composites is presented. In comparison to bulk nanocomposites, the CNTs are deposited solely onto the GF surface via an aqueous GF coating, making this approach independent of whether thermoplastic or thermoset resins are used as a matrix, respectively. The addition of dispersed CNTs to the coating formulation results in the

formation of CNT networks on the GF being capable of local strain mapping within the composites interphase.

The two main factors determining the electrical resistance of the coated GF yarns are the CNT weight fraction of the film former and the solid content of the film former/CNT system on the GF. If the coating content on the GF is below 10 wt% (appr. 30 vol%), the GF are inhomogeneously covered and characterized by a higher degree of discontinuous coating structures on the fibre surface, resulting in higher resistances. However, this percentage is specific for the system investigated and can be significantly lower, as it is mainly affected by the wettability of the GF by the chosen film former system.

Tensile testing in combination with simultaneous recording of the resistance for CNT-coated GF yarns embedded in a PP matrix, demonstrates the potential of interphase sensors for health monitoring of GF reinforced composites. The onset of GF breakage can be detected by a sudden increase in resistance. Moreover, by the slope of the resistance change curve indirect information about the interphase strain can be derived and critical loads regarding the interphase strength can be identified.

Acknowledgements

The authors are grateful for the support of this work by the Deutsche Forschungsgemeinschaft (DFG) within the framework of the collaborative research cluster SFB639 (subproject A1). Moreover, the authors wish to thank Dr. Pötschke for assistance with the resistivity measurements of the CNT-filled films. The help of Dr. Jenschke and Mr. Scheibner for experimental assistance is also greatly acknowledged.

References

[1] Measures RMM. Smart composite structures with embedded sensors. Comp Engin 1992;2(5-7):597-618.
[2] Rao YJ. Recent progress in applications of in-fibre Bragg grating sensors. Optics and Lasers in Engineering 1999;31(4):297-324.
[3] Zou Y, Tong L, Steven GP. Vibration-based model dependent damage (delamination) identification and health monitoring for composite structures – a review. J of Sound and Vibration 2000;230(2):357-378.
[4] Okabe Y, Mizutani T, Yashiro S, Takeda N. Detection of microscopic damages in compsite laminates with embedded small-diameter fibre Bragg grating sensors. Comp Sci Techn 2002;62(7-8):951-958.
[5] Zhou G, Sim LM. Damage detection and assessment in fibre-reinforced composite

structures with embedded fibre optic sensors - review. Smart Mater Struct 2002;11: 925–939.
[6] Zhongqing S, Lin Y, Ye L. Guided Lamb waves for identification of damage in composite structures: A review. J of Sound and Vibration 2006;295(3-5):753-780.
[7] Fiedler B, Gojny FH, Wichmann MHG, Bauhofer W, Schulte K. Can carbon nanotubes be used to sense damage in composites? Ann Chim-Sci Mat 2004;29(6):81–94.
[8] Park JM, Kim DS, Kim SJ, Kim PG, Yoon DJ, deVries KL. Inherent sensing and interfacial evaluation of carbon nanofiber and nanotube/epoxy composites using electrical resistance measurement and micromechanical technique. J Composites: Part B 2007;38(7-8):847-861.
[9] Wichmann MHG, Buschhorn ST, Böger L, Adelung R, Schulte K. Direction sensitive bending sensors based on multi-wall carbon nanotube/epoxy nanocomposites. Nanotechnology 2008;19:475503 (5pp).
[10] Thostenson ET, Chou TW. Carbon nanotube networks: sensing of distributed strain and damage for life prediction and self healing. Adv Mater 2006;18():2837-2841.
[11] Thostenson ET, Chou TW. Real-time *in situ* sensing of damage evolution in advanced fiber composites using carbon nanotube networks. Nanotechnology 2008;19:215713 (6pp).
[12] Böger L, Wichmann MHG, Meyer LO, Schulte K. Load and health monitoring in glass fibre reinforced composites with an electrically conductive nanocomposite epoxy matrix. Comp Sci Techn 2008;68(7-8):1886-1894.
[13] Li C, Thostenson ET, Chou TW. Sensors and actuators based on carbon nanotubes and their composites: A review. Comp Sci Techn 2008;68(6):1227-1249.
[14] Chou TW, Gao L, Thostenson ET, Zhang Z, Byun JH. An assessment of the science and technology of carbon nanotube-based fibers and composites. Comp Sci Techn 2010;70(1):1-19.
[15] Zhao Q, Wood JR, Wagner HD. Stress fields around defects and fibers in a polymer using carbon nanotubes as sensors. Appl Physics Letters 2001;78(12):1748-1750.
[16] Sureeyatanapas P, Young RJ. SWNT composite coatings as a strain sensor on glass fibres in model epoxy composites. CompSci Techn 2009;69(10):1547-1552.
[17] Sureeyatanapas P, Hejda M, Eichhorn SJ, Young RJ. Comparing single-walled carbon nanotubes and samarium oxide as strain sensors for model glass-fibre/epoxy composites. Comp Sci Techn 2010;70(1): 88-93.
[18] Kasaliwal G, Göldel A, Pötschke P. Influence of processing conditions in small-scale melt mixing and compression molding on the resistivity and morphology of polycarbonate–MWNT composites. J Appl Polym Sci 2009;112(6):3494-3509.
[19] Rausch J, Zhuang RC, Mäder E. Surfactant assisted dispersion of functionalized multi-walled carbon nanotubes in aqueous media. Composites A (2010), doi:10.1016/j.compositesa.2010.03.007
[20] Dufresne A, Paillet M, Putaux JL, Canet R, Carmona F, Delhaes P, Cui S. Processing and characterization of carbon nanotube/poly(styrene-co-butyl acrylate) nanocomposites. J Mat Sci 2002;37(18):3915-3923.
[21] Regev O, ElKati PNB, Loos J, Koning CE. Preparation of conductive nanotube-polymer composites using latex technology. Adv Mater 2004;16(3):248-251.
[22] Miltner HE, Grossiord N, Lu L, Loos J, Koning CE, Van Mele B. Isotactic

polypropylene/carbon nanotube composites prepared by latex technology. thermal analysis of carbon nanotube-induced nucleation. Macromolecules 2008; 41(15):5753-5762.

[23] Lu K, Grossiord N, Koning CE, Miltner HE, Mele B, Loos J. Carbon nanotube/isotactic polypropylene composites prepared by latex technology: morphology analysis of CNT-induced nucleation. Macromolecules 2008;41(): 8081-8085.

[24] Grossiord N, Loos J, van Laake L, Maugey M, Zakri C, Koning CE, Hart AJ. High-conductivity polymer nanocomposites obtained by tailoring the characteristics of carbon nanotube fillers. Adv Funct Mater 2008;18(20):3226-3234.

[25] Pegel, S, Pötschke P, Petzold G, Alig I, Dudkin SM, Lellinger D. Dispersion, agglomeration, and network formation of multiwalled carbon nanotubes in polycarbonate melts. Polymer 2008; 49(4):974-984.

[26] Ganß M, Satapathy BK, Thunga M, Weidisch R, Pötschke P, Jehnichen D. Structural interpretations of deformation and fracture behavior of polypropylene/multi-walled carbon nanotube composites. Acta Materialia 2008;56(10): 2247-2261.

[27] Villmow T, Pötschke P, Pegel S, Häussler L, Kretzmar B. Influence of twin-screw extrusion conditions on the dispersion of multi-walled carbon nanotubes in a poly(lactic acid) matrix. Polymer 2008;49(16):3500-3509.

[28] Bryning MB, Islam MF, Kikkawa JM, Yodh AG. Very low conductivity threshold in bulk isotropic single-walled carbon nanotube-epoxy composites. Adv Mater 2005;17(9):1186–91.

[29] Li J, Ma PC, Chow WS, To CK, Tang BZ, Kim JK. Correlations between percolation threshold, dispersion state, and aspect ratio of carbon nanotubes. Adv Funct Mater 2007;17(16):3207–3215.

[30] Gojny FH, Wichmann MHG, Köpke U, Fiedler B, Schulte K. Carbon nanotube-reinforced epoxy-composites - enhanced stiffness and fracture toughness at low nanotube contents. Compos Sci Technol 2004;64(15):2363–2371.

[31] Seo MK, Park SJ. Electrical resistivity and rheological behaviors of carbon nanotubes-filled polypropylene composites. Chem Phys Lett 2004;395(1-3):44–48.

[32] Tjong SC, Liang GD, Bao SP. Electrical behavior of polypropylene/multi-walled carbon nanotube nanocomposites with low percolation threshold. Scripta Mater 2007;57(6):461–464.

[33] Gorrasi G, Romeo V, Sannino D, Sarno M, Ciambelli P, Vittoria V, De Vivo B, Tucci V. Carbon nanotube induced structural and physical property transitions of syndiotactic polypropylene. Nanotechnology 2007;18(27):275703. 1-11.

[34] Micusík M, Omastová M, Krupa I, Prokes J, Pissis P, Logakis E, et al. A comparative study on the electrical and mechanical behaviour of multi-walled carbon nanotube composites prepared by diluting a masterbatch with various types of polypropylene. J Appl Polym Sci 2009;113(4):2536–2551.

[35] Wu HP, Wu XJ, Ge MY, Zhang GQ, Wang YW, Jiang JZ. Effect analysis of filler sizes on percolation threshold of isotropical conductive adhesives. Compos Sci Techn 2007; 67(6):1116–1120.

[36] Gojny FH, Wichmann MHG, Fiedler B, Kinloch I, Kinloch IA, Bauhofer W, et al. Evaluation and identification of electrical and thermal conduction mechanisms in carbon nanotube/epoxy composites. Polymer 2006;47(6):2036–2045.

[37] Yi YB, Berhan L, Sastry AM. Statistical geometry of random fibrous networks, revisited: waviness, dimensionality, and percolation. J Appl Phys

2004;96(3):1318–1327.
[38] Li CY, Thostenson ET, Chou TW. Effect of nanotube waviness on electric conductivity of carbon nanotube-based composites. Compos Sci Techn 2007;68(6):1445–1452.
[39] Li CY, Chou TW. Continuum percolation of nanocomposites with fillers of arbitrary shapes. Appl Phys Lett 2007;90(17):174108.
[40] Villmow T, Pegel S, Pötschke P, Wagenknecht U. Influence of injection molding parameters on the electrical resistivity of polycarbonate filled with multi-walled carbon nanotubes. Comp Sci Techn 2008;68(3-4):777-789.
[41] Bauhofer W, Kovacs JZ.A review and analysis of electrical percolation in carbon nanotube polymer composites Comp Sci Techn 2009;69(10):1486-1498.
[42] Oatley CW, Everhart TE. The examination of p–n junctions with the SEM, J Electron 1957;2(6):568–570.
[43] Chung KT, Reisner JH, Campbell ER. Charging phenomena in the scanning electron microscopy of conductor–insulator composites: a tool for composite structural analysis, J Appl Phys 1984;54(11):6099–6112.
[44] Loos J, Alexeev A, Grossiord N, Koning CE, Regev O, Visualization of single-wall carbon nanotube (SWNT) networks in conductive polystyrene nanocomposites by charge contrast imaging, Ultramicroscopy 2005;104(2):160-167.
[45] Kovacs JZ, Andresen K, Pauls JR, Garcia CP, Schossig M, Schulte K, Bauhofer W. Analyzing the quality of carbon nanotube dispersions in polymers using scanning electron microscopy. Carbon 2007;45(6):1279-1288.
[46] Zinck P, Pays MF, Rezakhanlou R, Gerard JF. Mechanical characterisation of glass fibres as an indirect analysis of the effect of surface treatment. J Mater Sci 1999;34(9):2121-2133.

Figure captions

Figure 1: Scheme of specimen for tensile testing and simultaneous recording of resistance change of the CNT- coated GF yarn embedded in a PP matrix

Figure 2: Volume resistivity as a function of CNT weight fraction of nanocomposites prepared by adding pre-dispersed CNTs to an aqueous film former system

Figure 3: SEM micrographs of GF with CNT-coating. The solid content on the GF is 5.5 wt%. a) as-coated GF with patchy coverage of GF surface by CNT-coating b) higher magnification of the as-coated GF showing dispersed CNTs within the spherically shaped PP particles of the film former, c) surfaces of GF after annealing at 200°C for 15 min, d) charge contrast SEM image of CNT-coating on a GF after annealing at 200°C for 15 min

Figure 4: Schematical views of differently coated GF. Red areas indicate the CNT/film former system.a) cross section of an ideally coated GF. The coating forms a homogeneous and thin layer on the whole GF surface; b) Ideally coated GF surface, characterized by a continuous and thin coating layer stretching out on the whole GF surface; c) cross section of an coated GF, showing inhomogeneities in the coating distribution and coating layer thickness; d) GF surface, showing an irregular coating pattern where certain parts of the coated surface are not connected to the continuously coated area providing a conductive path on the GF surface

Figure 5: Dependence of resistance of CNT-coated GF on the yarn length for different coating contents. Linear lines show least square fit through the origin of the resistance data and the corresponding slopes

Figure 6: Calculated volume resistivity of CNT-coated GF yarns for different coating weight fractions and various yarn lengths

Figure 7: Stress displacement curve and simultaneous recording of the resistance change for a GF yarn embedded in PP matrix. CNT-coating weight fraction of the yarn is 14.5 %. R_0 for the sample is 494 kOhm

Tables

Table 1: Resistance data of GF yarns for different coating contents as a function of yarn length and slope of linear least square fit (cf. fig. 3) for the resistance data of differently coated GF yarns

	resistance [Ohm]								
coating content of GF yarn [wt%]	5 cm	standard deviation	10 cm	standard deviation	20 cm	standard deviation	30 cm	standard deviation	slope *m* of *y=m*x* [Ohm]
5.5	1.47E+07	6.01E+06	3.01E+07	9.10E+06	5.84E+07	1.31E+07	8.62E+07	2.11E+07	2.92E+06
10.4	1.74E+06	1.73E+05	3.53E+06	4.94E+05	7.11E+06	4.70E+05	1.08E+07	4.82E+05	3.58E+05
14.5	8.98E+05	1.53E+05	1.85E+06	1.84E+05	3.64E+06	2.76E+05	5.49E+06	4.03E+05	1.83E+05
21.6	5.93E+05	3.97E+04	1.22E+06	7.31E+04	2.41E+06	1.04E+05	3.65E+06	2.28E+05	1.21E+05
29.4	3.56E+05	3.07E+04	7.53E+05	6.54E+04	1.56E+06	2.67E+05	2.38E+06	3.88E+05	7.64E+04

Figures

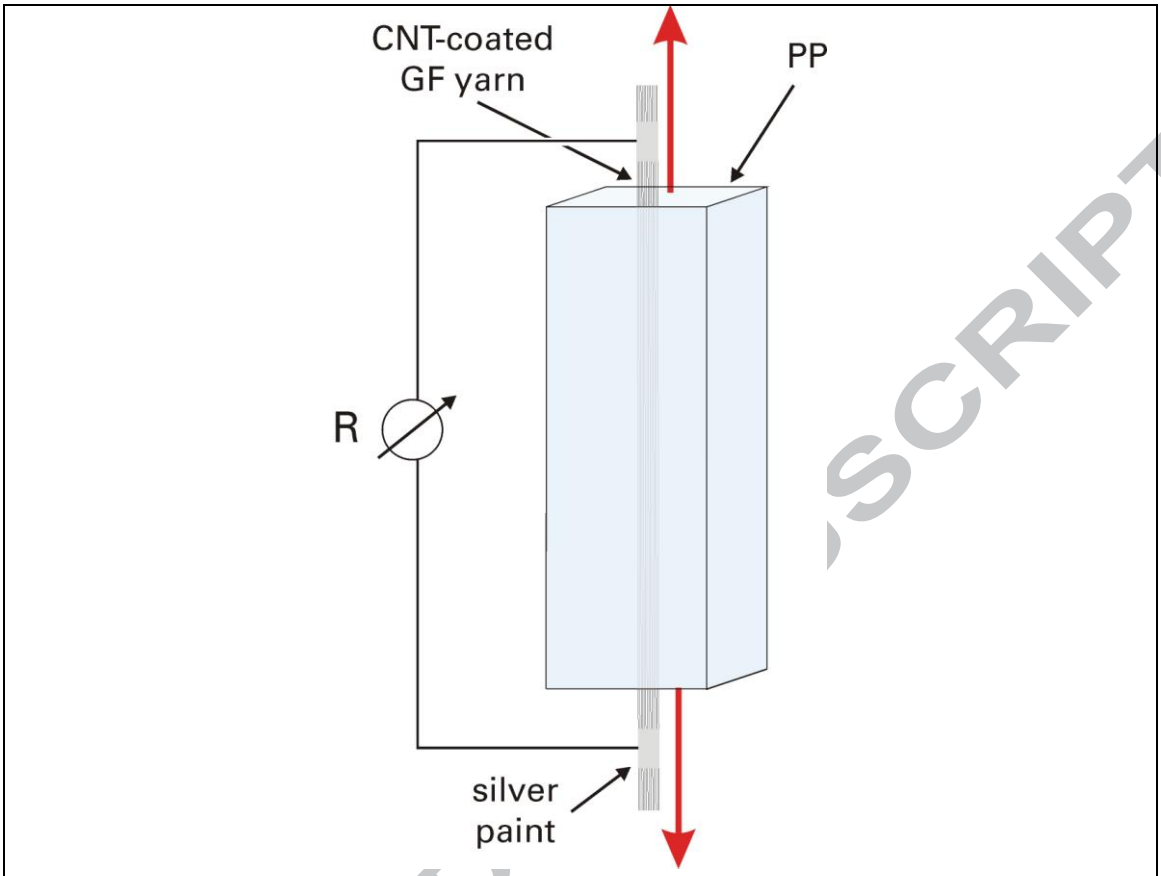

Figure 1: Scheme of specimen for tensile testing and simultaneous recording of resistance change of the CNT-coated GF yarn embedded in a PP matrix

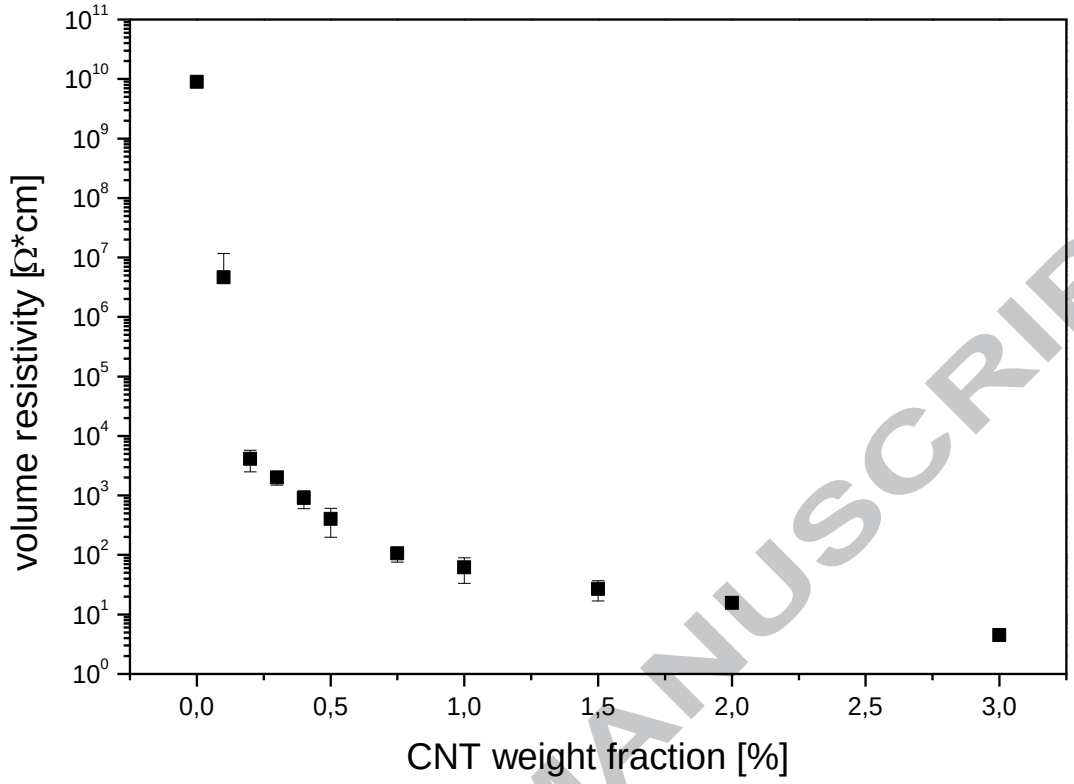

Figure 2: Volume resistivity as a function of CNT weight fraction of nanocomposites prepared by adding pre-dispersed CNTs to an aqueous film former system

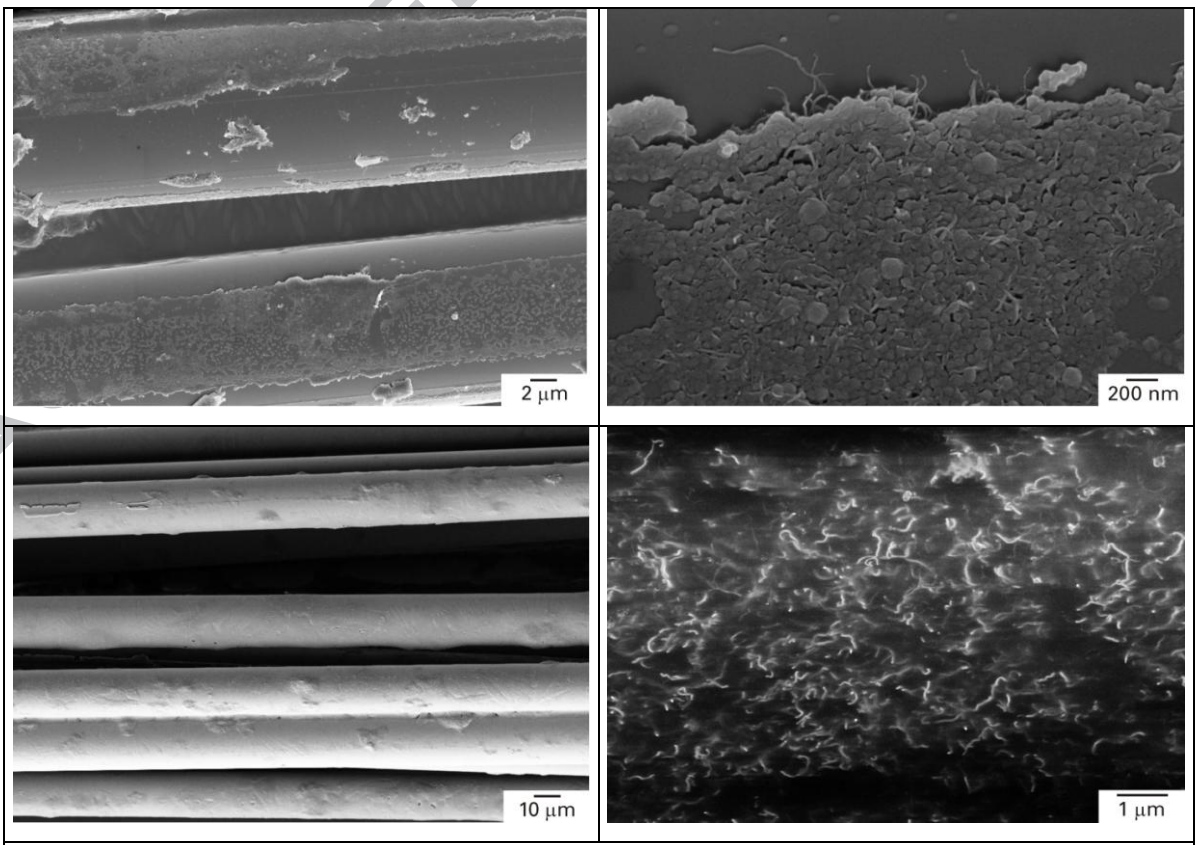

Figure 3: SEM micrographs of GF with CNT-coating. The solid content on the GF is 5.5

wt%. a) as-coated GF with patchy coverage of GF surface by CNT-coating b) higher magnification of the as-coated GF showing dispersed CNTs within the spherically shaped PP particles of the film former, c) surfaces of GF after annealing at 200°C for 15 min, d) charge contrast SEM image of CNT-coating on a GF after annealing at 200°C for 15 min

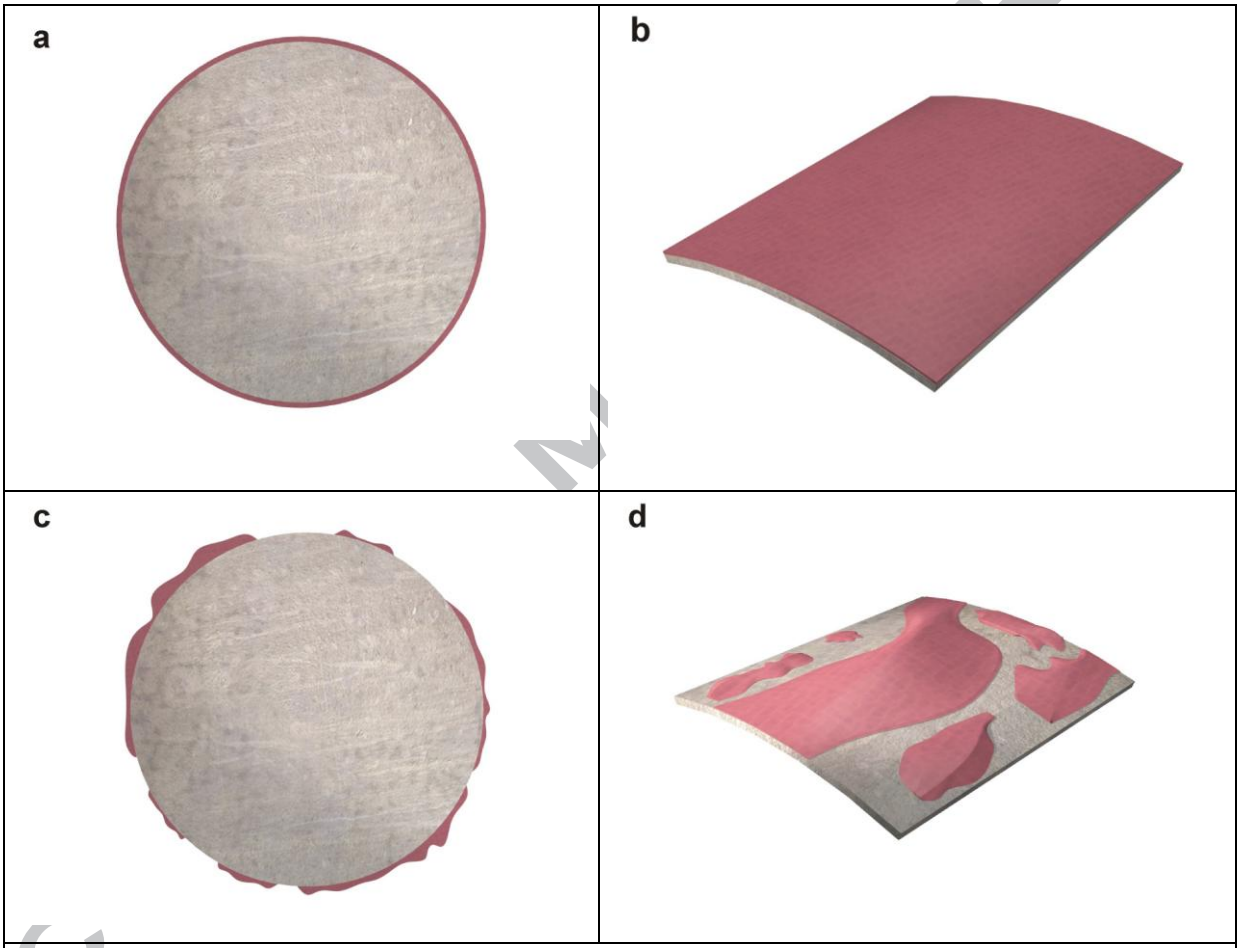

Figure 4: Schematical views of differently coated GF. Red areas indicate the CNT/film former system. a) cross section of an ideally coated GF. The coating forms a homogeneous and thin layer on the whole GF surface; b) Ideally coated GF surface, characterized by a continuous and thin coating layer stretching out on the whole GF surface; c) cross section of an coated GF, showing inhomogeneities in the coating distribution and coating layer thickness; d) GF surface, showing an irregular coating pattern where certain parts of the coated surface are not connected to the continuously coated area providing a conductive path on the GF surface

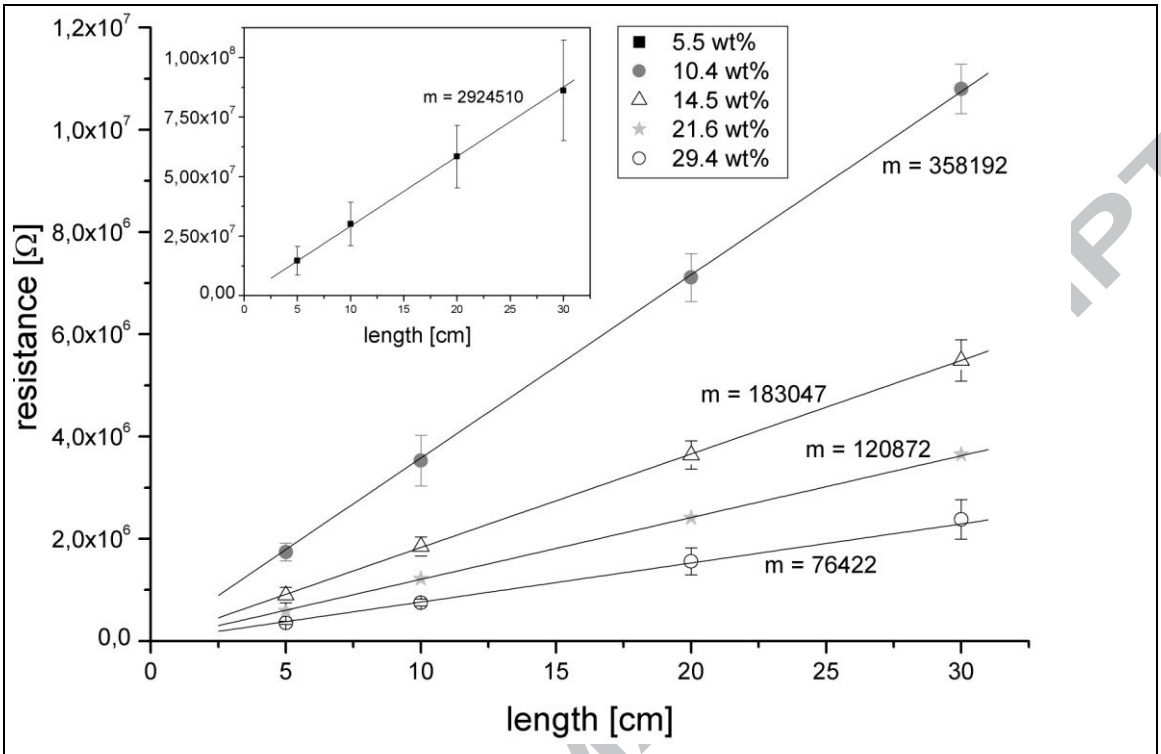

Figure 5: Dependence of resistance of CNT-coated GF on the yarn length for different coating contents. Linear lines show least square fit through the origin of the resistance data and the corresponding slopes

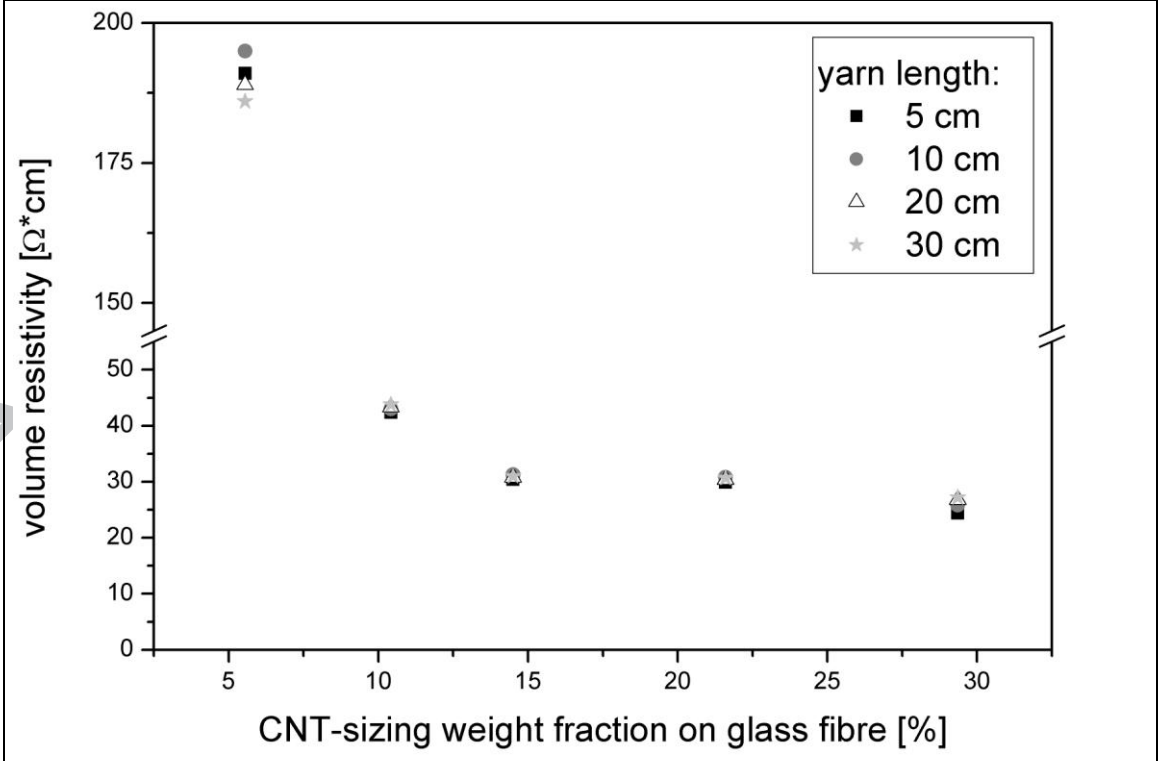

Figure 6: Calculated volume resistivity of CNT-coated GF yarns for different coating weight fractions and various yarn lengths

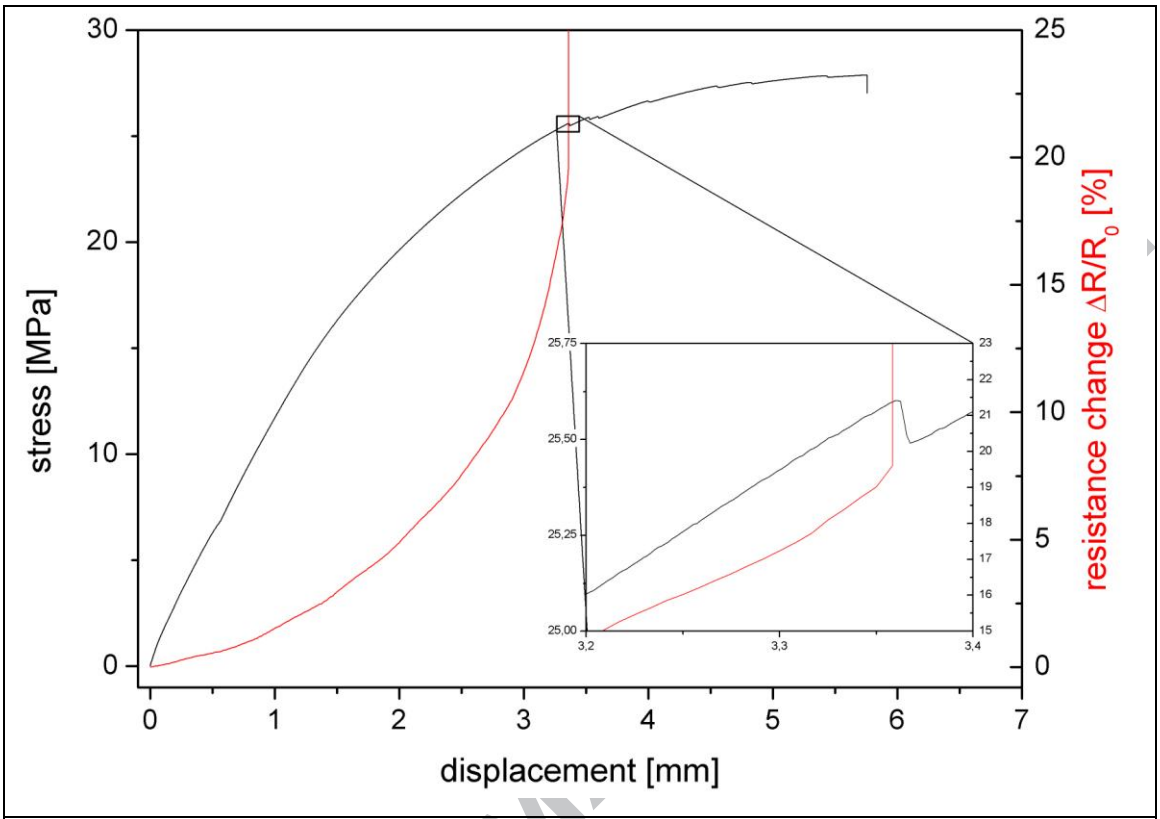

Figure 7: Stress displacement curve and simultaneous recording of the resistance change for a GF yarn embedded in PP matrix. CNT-coating weight fraction of the yarn is 14.5 %. R_0 for the sample is 494 kOhm